Electronic Delivery Cover Sheet

PERGAMON

Engineering Fracture Mechanics 70 (2003) 309–337

Engineering Fracture Mechanics

www.elsevier.com/locate/engfracmech

Effect of loading and geometry on the subsonic/intersonic transition of a bimaterial interface crack

O. Samudrala, A.J. Rosakis *

Graduate Aeronautical Laboratories, California Institute of Technology, Mail stop 105-50, Pasadena, CA 91125, USA

Received 6 September 2001; received in revised form 5 February 2002; accepted 12 February 2002

Abstract

An experimental investigation was conducted to study the nature of intersonic crack propagation along a bimaterial interface. A single edge notch/crack oriented along a polymer/metal interface was loaded predominantly in shear by impacting the specimen with a high velocity projectile fired from a gas gun. The stress field information around the propagating crack tip was recorded in real time by two different optical techniques—photoelasticity and coherent gradient sensing, in conjunction with high speed photography. Intersonic cracks on polymer/metal interfaces were found to propagate at speeds between the shear wave speed (c_s) and $\sqrt{2}c_s$ of the polymer. The nature of the crack tip fields during subsonic/intersonic transition and the conditions governing this transition were examined. Experimental observations showed the formation of a crack face contact zone as the interfacial crack speed exceeds the Rayleigh wave speed of the polymer. Subsequently, the contact zone was observed to expand in size, shrink and eventually collapse onto the intersonic crack tip. The recorded isochromatic fringe patterns showed multiple Mach wave formation associated with such a scenario. It is found that the nature of contact zone formation as well as its size and evolution differ substantially depending on the sign of the opening component of loading.

Keywords: Bimaterial; Dynamic fracture; Mach waves; Frictional contact; Intersonic speeds

1. Introduction

Many modern engineering materials like fiber/whisker/particle-reinforced polymer composites, metal–matrix composites, polycrystalline intermetallic alloys, structural ceramics and others contain interfaces joining two dissimilar materials. In addition, many engineering components like thin-film/substrate systems, laminates, multilayer capacitors, reaction–product layers, protective coatings, photovoltaic cells, soldered joints, adhesive joints, human joint replacements, piezoelectric actuators, welds and numerous others also feature material interfaces. Frequently these interfaces contain flaws due to imperfect bonding, residual stresses etc. Even otherwise, the mismatch in elastic and thermal properties across the interface leads to stress concentration and consequently becomes a favored site for flaw initiation during normal

* Corresponding author. Tel.: +1-626-395-4523; fax: +1-626-449-6359.
E-mail address: rosakis@aero.caltech.edu (A.J. Rosakis).

0013-7944/03/$ - see front matter
PII: S0013-7944(02)00025-5

operating cycles. As such interface failure in these materials is a common occurrence, caused due to the propagation and coalescence of preexisting or nucleated cracks along the interface. Hence an understanding of the mechanics of interface failure is essential to gauge the efficiency and reliability of such materials/components.

Interface cracks can initiate under either quasi-static or dynamic loading conditions. However, the eventual decohesion frequently proceeds in a catastrophic manner. From a practical point of view, the main interest in interface fracture is towards predicting the initiation of a preexisting crack, however, there are numerous instances where dynamic crack propagation is of interest, especially for predicting crack arrest, for assessing and minimizing damage caused due to catastrophic failure and so on. Appropriate dynamic failure criteria are essential in obtaining accurate numerical simulations of the macroscopic response of multi-phase materials under dynamic loading. The potential applications where an understanding of dynamic crack propagation is profitable are summarized in an article by Kanninen and O'Donoghue [1]. Dynamic interfacial rupture is also of great importance in modeling earthquake source processes [2–9].

An in-plane crack on a dissimilar material interface generally experiences a mixed-mode deformation in the tip vicinity, even though the applied far-field loading possesses the symmetries of a pure mode. Similar to a crack in a homogeneous solid, a bimaterial interface crack also opts, if possible, to kink into one of the materials on either side and to establish pure mode I conditions near the tip. However, if one of the phases has a higher fracture toughness than the other, an interface crack under certain far-field mode mixities might prefer to propagate along the interface itself even though this interface may not be significantly weaker than both phases. Hence, the possibility of mixed-mode and in particular, shear dominated crack propagation is much more pronounced along a dissimilar material interface than in homogeneous solids. The theory of kinking of a crack out of an interface was thoroughly explored in the articles by He and Hutchinson [10], He et al. [11] and has been reviewed by Hutchinson and Suo [12].

Dynamic crack propagation along an interface separating two dissimilar, homogeneous, isotropic, linear elastic solids has received attention only in the past decade. After a few initial analytical investigations, [13–17] interest in the area subsided due to the lack of supporting experimental observations. In the first (to author's knowledge) systematic experimental investigation on dynamic crack propagation along a bimaterial interface, Tippur and Rosakis [18] observed interfacial cracks along polymethylmethacrylate (PMMA)/6061 aluminum interfaces propagating at speeds close to 80% of the Rayleigh wave speed of PMMA (c_R^{PMMA}) and featuring accelerations as high as 10^7 g. In contrast, cracks in homogeneous PMMA rarely exceed 35% of c_R^{PMMA}, before branching into multiple cracks. The observation that a PMMA/Al interface can sustain much higher crack speeds spurred a renewal of interest in dynamic crack propagation along bimaterial interfaces. Hereafter, whenever the superscript on a material property is omitted, it is assumed that it represents the property corresponding to that of the constituent with the lower wave speeds. Yang et al. [19] obtained explicit expressions for the dominant stress field around a crack running subsonically (subsonic with respect to the half with lower wave speeds) along a bimaterial interface. Based on experimental observations, Lambros and Rosakis [20,21] and Kavaturu and Shukla [22] proposed propagation criteria for subsonic crack growth along a bimaterial interface. Lambros and Rosakis [20] proposed that the crack face profile remains unchanged during subsonic interfacial crack propagation, whereas Kavaturu and Shukla [22] proposed that crack face displacement components increase with crack speed according to a power law. An interesting feature exhibited by both these criteria is that the dynamic fracture toughness decreases as the lower of the two Rayleigh wave speeds is approached. This behavior is opposite to that observed in homogeneous polymers and metals (in the absence of favorable crack paths) where the dynamic fracture toughness is usually observed to increase sharply with crack speed as the crack accelerates close to the onset of the branching instability. Rosakis and coworkers [23–26] and Singh and Shukla [27] demonstrated experimentally that under highly shear dominated conditions, bimaterial interface crack speeds can exceed c_s of the material with lower wave speeds and become intersonic (with respect to half with lower wave speeds). Motivated by these observations, Huang et al. [28,29] and Yu and Yang [30,31] derived

the asymptotic near-tip fields for an intersonic crack on a bimaterial interface and showed that some of the features observed in the experimental fringe patterns are predicted by the analytical solution. More recently, Yu and Suo [32] and Brock [33,34] obtained general solutions for the near tip fields around an interface crack propagating at a constant speed in orthotropic or transversely isotropic bimaterials.

As observed experimentally and predicted analytically, the stress field distribution around an intersonic crack on a bimaterial interface differs dramatically from that around a subsonic interfacial crack. Since the crack speed has exceeded c_s of the half with lower wave speeds, all the shear waves generated by the running crack in the half with lower wave speeds are restricted to lie behind a Mach wave radiating from the crack tip. The Mach wave carries with it a strong discontinuity in stress field. Such a Mach wave was first predicted by Liu et al. [28] and was subsequently observed in the isochromatic fringe patterns recorded by Singh and Shukla [27]. In addition to the Mach wave radiating from the tip, they also observed a second Mach wave parallel to the first one and radiating from a point, a finite distance behind the tip. This observation was consistent with the earlier conjecture by Lambros and Rosakis [24] who proposed, on the basis of the shape of CGS interferograms, that an intersonic crack on a bimaterial interface propagates with a finite zone of crack face frictional contact behind it. The observation of a second Mach wave in the isochromatic fringes provided further evidence of finite contact and explained the finite separation distance between the two lobes of the CGS fringe pattern on either side of the intersonically moving crack tip [24]. The size of the contact zone was found to be of the order of a few millimeters. Motivated by this observation, Huang et al. [35] and Wang et al. [36] obtained the near-tip fields around an intersonically propagating interfacial crack with a finite zone of crack face frictional contact behind the tip. Numerical simulations also showed that intersonic interfacial crack propagation is accompanied often by non-uniform, large scale crack face contact zones and lines of stress field discontinuity [37–39]. The transient mechanism governing the formation of this large-scale crack face contact zone as the interfacial crack accelerates from subsonic to intersonic speeds is rather obscure. Indeed, the effect of loading geometry (e.g. sign of shear) and of confining pressure on the nature of large scale contact has not been investigated in detail. The structure of the contact zone as well as its evolution history during the entire intersonic crack growth process are some of the issues pursued in this work.

2. Specimen configuration and experimental procedure

The primary goal of the experiments is to investigate the nature of intersonic crack propagation along bimaterial interfaces. The experimental procedures used for this investigation closely parallel those adopted by Tippur and Rosakis [18] and Singh and Shukla [27]. Polymer/metal adhesive joints were chosen to model bimaterial interfaces with strong wave speed mismatch. Dynamic crack growth was induced along the bond line by impacting the specimen with a projectile fired from a high-speed gas gun. To extract stress field information around the propagating crack, two different full-field optical techniques were used—photoelasticity and coherent gradient sensing (CGS) interferometry. The resulting fringe patterns were recorded in real time using high-speed photography.

The specimens for investigating dynamic crack growth along a dissimilar material interface were made by bonding two plates of identical dimensions, one of polymer, either Homalite or PMMA, and the other of metal, either 6061-T6 aluminum alloy or SAE-AISI 4340 Steel (see Fig. 1). Each half of the bimaterial specimens was 150 mm long, 125 mm wide and either 6.4 or 9.5 mm thick. A few bimaterial specimens with each half 250 mm long, 50 mm wide and 9.5 mm thick were also tested to investigate the influence of specimen geometry. The polymers were chosen for their suitability to apply particular optical techniques for stress analysis. Homalite when stressed becomes optically birefringent, which permits the use of photoelasticity for stress analysis. PMMA is optically isotropic and transparent. CGS interferometry in transmission configuration is used for extracting stress field information in PMMA. Both Homalite and PMMA

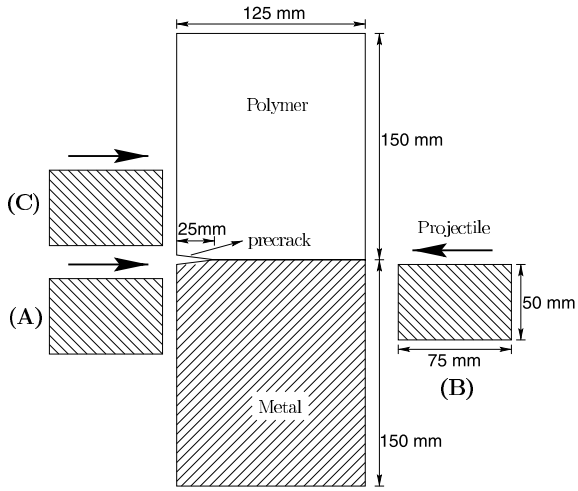

Fig. 1. Bimaterial specimen with a precrack subjected to impact shear loading, (A), (B) and (C) show the three different impact configurations tested.

are brittle and exhibit a linear elastic behavior at room temperature and at the rates of loading experienced in the experiments. Metals were chosen to be the second halves of the bimaterial, since they provide a strong wave speed and stiffness mismatch across the interface, mimicking the scenario encountered in composites. The mechanical and optical properties of relevance for the specimen materials are given in Table 1.

Both the polymeric materials, Homalite and PMMA exhibit rate sensitivity with regard to their elastic wave speeds and elastic moduli. The static values given in Table 1 correspond to a strain rate of the order 10^{-3} s^{-1}, where as the dynamic values correspond to a strain rate of the order 10^{3} s^{-1} [25]. In general, the material surrounding a propagating crack experiences a wide spectrum of strain rates and in the tip vicinity the strain rates experienced by the material particles usually fall in the dynamic range. Hence for the material in the vicinity of a propagating crack tip, the dynamic values of the material properties are more relevant. The static values of E and v for the polymers shown in Table 1 were taken from [25] and the rest of

Table 1
Material property chart

Property	PMMA		Homalite-100		6061 Aluminum	4340 Steel
	Static	Dynamic	Static	Dynamic		
Young's modulus, E (GPa)	3.2	5.9	3.9	5.2	74.2	213.1
Shear modulus, μ (GPa)	1.2	2.2	1.4	1.9	27.8	82.9
Poisson's ratio, v	0.35	0.33	0.35	0.34	0.34	0.29
Density, ρ (kgm^3)	1190		1230		2710	7830
Shear wave speed, c_s (m/s)	998	1363	1084	1255	3200	3254
Longitudinal wave speed (plane strain), $c_l^{pl-\sigma}$ (m/s)	2078	2715	2256	2558	6445	5935
Longitudinal wave speed (plane stress), $c_l^{pl-\sigma}$ (m/s)	1751	2358	1901	2187	5555	5443
Rayleigh wave speed (plane strain), $c_R^{pl-\epsilon}$ (m/s)	933	1271	1014	1172	2986	3010
Rayleigh wave speed (plane stress), $c_R^{pl-\sigma}$ (m/s)	919	1253	998	1155	2943	2977

From [53].

the elastic properties were calculated using the standard relations for an isotropic linear elastic solid. The dynamic values of the elastic wave speeds, $c_l^{\mathrm{pl}-\epsilon}$ and c_s were measured by a pulse-echo technique using a 10 MHz transducer on an ultrasonic analyzer. The dynamic moduli and other elastic properties are calculated from these measured values. Both the metals, 6061 aluminum and 4340 steel do not exhibit any appreciable strain rate sensitivity. The material properties for aluminum are taken from ASM handbook and those of steel were obtained from the manufacturer.

The bonding surface on the polymer halves was roughened by mechanical abrasion with 220 grit sand paper. The metal halves were blanchard ground to the desired thickness and the bonding surfaces were surface ground to obtain a flat profile. The bonding surface on the metal halves was roughened uniformly by bead blasting with glass beads of 10–20 μm diameter. The specimen halves were cleaned thoroughly using isopropyl alcohol (for polymers) and acetone (for metals) prior to bonding. The bonding agents were chosen carefully so that the constitutive properties of the bond are close to those of the polymer, thus avoiding the introduction of a new material. For PMMA/metal bimaterial specimens, methylmethacrylate monomer was chosen to be the adhesive with the appropriate catalyst for polymerization. For Homalite/Homalite and Homalite/metal specimens, unplasticized polyester resin was chosen as the adhesive with the appropriate hardener and accelerator. The bonding agent was prepared by mixing the constituents in appropriate ratio by weight. It is applied uniformly to the two surfaces, which are then aligned and held under pressure in a specially designed fixture. After about 48 h at room temperature the curing of the bond is complete. The thickness of the bond obtained using the above procedure was about 100 μm and about 20–30 μm for the methylmethacrylate adhesive and polyester resin adhesive respectively. The bimaterial specimens have either a precut edge notch or a sharp edge precrack, 25 mm long along the interface. To introduce a precrack, a thin teflon tape or machine grease was used to prevent bonding over a 25 mm region starting from one end. In some of the bimaterial specimens, a blunt notch, 25 mm long was machined using a band saw, starting from one end. Adequate care was taken to ensure that the notch is centered along the interface. The notch width was dictated by the width of the band saw, which was approximately 750 μm.

Tippur and Rosakis [18], Lambros [40] and Singh [41] performed calibration tests for bonds obtained using the above procedure. Additional tests were also performed to obtain the tensile strength and shear strength of PMMA/PMMA and Homalite/Homalite adhesive bonds. It was found that the strength of the bond can vary substantially depending on the relative proportions of the adhesive constituents, surface roughness, curing time and rate of loading. These tests show that irrespective of the bonding procedure followed, the bond line is always weaker than the monolithic material itself and hence often forms a preferred path for crack propagation. Also the tensile and shear strengths of the bonds under quasi-static loading rates (calibration test conditions) may vary significantly from those at the dynamic loading rates experienced by the bond during dynamic crack propagation.

Two different optical techniques were used to record, in real time, the stress field information around a propagating crack. For Homalite/Homalite specimens and Homalite/metal specimens, dynamic photoelasticity was used, whereas for PMMA/metal bimaterial specimens, CGS interferometry was used. Both these techniques are complimentary, in the sense that the information about the stress field provided by these techniques is different. Whereas photoelasticity provides information about the local maximum in-plane shear stress, CGS interferometry provides information about the gradient (in the shearing direction) of the sum of in-plane normal stresses at the point. The theory of photoelasticity is thoroughly explored by Dally and Riley [42] and CGS interferometry is explained in detail by Rosakis [43].

Fig. 2 shows a typical experimental setup for dynamic photoelasticity experiments. A more detailed illustration of the specimen geometry was shown in Fig. 1 along with all the relevant dimensions. This specimen geometry is a simplified version of the one introduced by Kalthoff [44] for investigating crack behavior under dynamic shear loading. The specimen is loaded dynamically by impacting it with a projectile fired from a high-speed gas gun. A compressive longitudinal loading pulse results which loads the

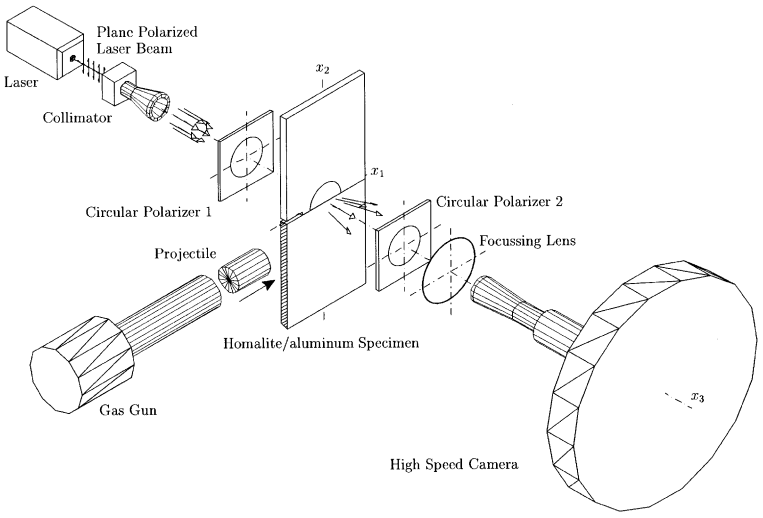

Fig. 2. Dynamic photoelasticity setup showing a Homalite/aluminum specimen placed inside a circular polariscope and being subjected to impact shear loading by a projectile fired from a high speed gas gun. The resulting isochromatic fringe patterns are recorded by high speed photography.

crack/notch tip predominantly in a shearing mode. The gas gun has a 2200 mm long steel barrel and fires a 75 mm long, 50 mm diameter cylindrical projectile made of hardened steel. Compressed air at 80–550 KPa was used as the driving medium which resulted in projectile velocities ranging from 8 to 40 m/s.

An Innova Sabre argon-ion pulsed laser was used as the light source in our experiments. The laser was set to operate on a single wave length—514.5 nm (blue-green light). At this wave length the continuous (CW) power output of the laser is 8 W. The laser emits an intense beam of 2 mm diameter which is 100:1 vertically polarized. An acousto-optic modulator (Bragg cell) is placed in front of the laser to produce a pulsed output. The duration of each laser pulse can be varied between 8 and 20 ns. Such short exposure times are required to prevent blurring and to record a sharp image on the film. During the actual experiment, the acousto-optic modulator is driven by the high-speed camera to control the timing of each laser pulse, so that it coincides with the time the camera optics are aligned to expose a particular frame on the film track. An electromechanical shutter is placed in front of the laser to prevent the light "leaking" through the Bragg cell from exposing the film. A wide gap sensor mounted on the gas gun barrel, about 30 mm from the end, is used to trigger the shutter open for a short duration ($\approx$10 ms) during the event. A strain gage bonded to the specimen at the impact site is used to trigger recording by the high-speed camera on impact. The coherent, monochromatic, plane polarized light output by the laser is collimated to a beam of 50 mm diameter. The laser beam is transmitted through the specimen placed inside a circular polariscope or a CGS interferometer and the resulting fringe pattern is recorded by a high speed camera. For bimaterial specimens, the metal half being opaque, only one half of the beam is transmitted through the specimen.

A Cordin model 330A rotating mirror type high-speed film camera was used to record the instantaneous fringe patterns generated by either of the two optical techniques mentioned above. The high-speed camera records 80 distinct frames at framing rates of up to 2 million frames per second. A feedback signal from the turbine is fed to a 10 Khz frequency counter which allows a precise monitoring of the turbine speed. Also the synchronizing signal sent by the camera to the acousto-optic modulator is simultaneously routed to a HP digital oscilloscope to obtain a record of the timings of each individual laser pulse. In this experimental work, most of the high-speed photography was performed at 720,000 frames per second, resulting in a frame every 1.4 μs.

In our experiments, the conditions governing the acceleration of a bimaterial interface crack to intersonic speeds are examined, with particular attention being focused on recording the subsonic/intersonic transition and evolution of the finite crack face contact zone discussed in Section 1. The effect of different loading configurations and specimen geometries on the attainment of intersonic crack speeds and on the propagation behavior of the interfacial crack is investigated. Four different material combinations were used in our bimaterial experiments—Homalite/Al, Homalite/steel, PMMA/Al and PMMA/steel. The essential details regarding specimen preparation and the experimental procedure were summarized above. The bimaterial specimen was subjected to in-plane loading and the three different loading configurations (A), (B) and (C) (see Fig. 1) essentially resulted in widely varying "mixities" at initiation. Impacting the specimen on the Homalite half on the side opposite the precrack/notch, resulted in cracks initiating from the impact site much earlier compared to the initiation of the edge crack on the opposite side. Hence this particular loading configuration was not pursued. The loading configuration (A) always resulted in a crack initiating from the edge precrack/notch at a steep angle to the interface and propagating into the polymer half. The other two loading configurations (B) and (C) resulted in interfacial crack propagation at intersonic speeds. However, the nature of the near-tip fields and propagation characteristics in either of these two cases were different, as explained later.

3. Kinking of a crack from a bimaterial interface

Loading an edge precrack/notch on a bimaterial interface under loading configuration (A) (see Fig. 1) always resulted in the initiation of a kinked crack (from the edge precrack/notch tip) at a steep angle to the interface and propagating into the polymer half. Specimens were loaded by impacting with cylindrical steel projectiles at speeds ranging from 10 to 35 m/s. Fig. 3 shows a selected sequence of four isochromatic fringe patterns depicting such an event. An edge precrack along a Homalite/Al interface was loaded by projectile impact, which resulted in the initiation and propagation of a kinked crack, inclined at an angle of $\approx 70°$ to the interface ahead. The projectile impact speed was 25.9 m/s and the semicircular field of view of diameter 50 mm was centered on the interface, 21.6 mm ahead of the precrack tip. The time elapsed from impact is shown on each frame. Fig. 3(a) shows the precrack being loaded by stress waves from the impact site, Fig. 3(b) shows the initiation of the kinked crack and in Fig. 3(c) and (d) we can see the kinked crack propagating into the Homalite half at a low subsonic speed of $0.4c_s$. The theory governing the kinking of a stationary crack on a bimaterial interface was discussed in Hutchinson and Suo [12] and He et al. [10,11,45]. It is quite likely that under certain combinations of interface fracture toughness and strength, intensity of applied load and the load phase angle, the precrack might initiate and propagate along the interface.

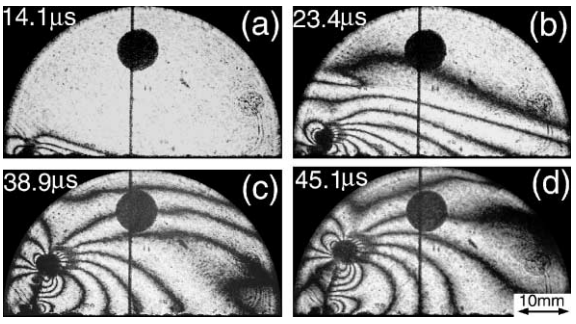

Fig. 3. Kinking of a crack from a Homalite/aluminum interface. A kinked crack at 69.8° to the interface resulted from impacting a bimaterial specimen on the metal half, on the same side as the starter crack. Impact speed of the projectile, $V = 25.9$ m/s and the semicircular field of view of 50 mm diameter was centered on the interface 21.6 mm ahead of the crack tip.

However in our specimens, for the range of projectile impact speeds mentioned above and with a loading configuration (A), interfacial failure never occurred. The competition between crack advance within the interface and kinking out of the interface depends on the relative toughness of the interface to that of the adjoining material. The bimaterial interface toughness is not a single material parameter, but rather it is a strong function of the near-tip mode mixity ψ (associated with a reference length L) [46,47], apart from being a function of loading rate (under dynamic loading only). This could possibly explain why interface crack growth was obtained under this loading configuration along a weak plane between two Homalite halves [48], but not on a polymer/metal interface.

4. Initiation and propagation of intersonic cracks on a bimaterial interface under loading configuration (B)

Loading an edge precrack/notch on a bimaterial interface under loading configuration (B) (see Fig. 1) always resulted in the initiation and propagation of an interface crack at intersonic speeds. Fig. 4 shows a selected sequence of eight isochromatic fringe patterns depicting the initiation of a precrack on a Homalite/aluminum interface and propagating along it. The time elapsed from impact and the crack tip speed (after initiation) are shown in each frame. The speed of the projectile, V, at impact was 9.6 m/s and the roughly semicircular field of view of 50 mm diameter was centered on the interface, 19.5 mm ahead of the precrack tip. In Fig. 4(a) and (b) we see the transmission of loading waves from the metal half into the polymer half through the interface and in Fig. 4(c) we can see that the precrack has just initiated. From Fig. 4(d) and (e) we see that the initiated crack quickly accelerates to speeds beyond c_R of the polymer within 7–8 μs after

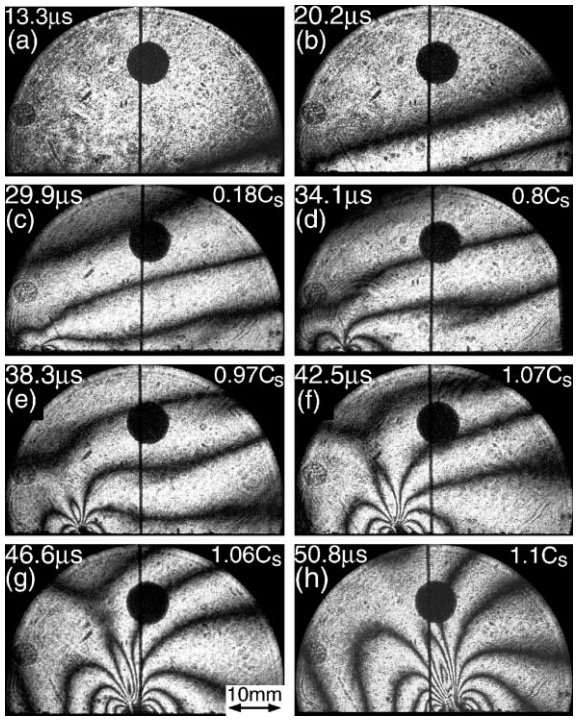

Fig. 4. Initiation and acceleration to intersonic speeds of a crack on Homalite/aluminum interface under impact shear loading. Impact speed, $V = 9.6$ m/s. The semicircular field of view of 50 mm diameter is centered on the interface 19.5 mm ahead of the initial precrack tip.

initiation. Crack speed acceleration during this phase is as high as 10^8–10^9 m/s^2. From Fig. 4 (f)–(h) we can see that the propagating interface crack attains intersonic speeds, even though it propagates at a speed only slightly above c_s. The size of the isochromatic fringe pattern increases, reflecting the increase in magnitude of the crack tip fields due to the increase in crack length.

To observe the interface crack behavior as it propagated further away from the initial precrack tip, the field of view of 50 mm diameter was moved further down stream along the interface. Fig. 5 shows a selected sequence of eight isochromatic fringe patterns around an intersonic interfacial crack propagating on a Homalite/Al interface. Again the time elapsed from impact and crack speed are shown in each frame. In this experiment, speed of projectile at impact was 9.9 m/s and the field of view of 50 mm diameter was centered on the interface, 37 mm ahead of the initial precrack tip. We see that once the interface crack accelerates quickly to intersonic speeds, it continues to propagate at an almost constant speed varying between c_s and $1.2c_s$. However, the nature of the isochromatic fringe pattern around the propagating intersonic crack tip is observed to undergo very dramatic changes. We see from Fig. 5(b) that the crack tip region is no longer the sharp point of isochromatic loop convergence, but has a more diffuse structure as noticed from the fact that the two lobes of the isochromatic fringe pattern around the tip are separated by a finite distance. In Fig. 5(e) and (f) we can see sharp lines radiating from the crack tip region into the polymer half. These are the traveling Mach waves (see Section 1) which delineate the extent of propagation of shear disturbances emanating from the tip region. Across these Mach waves the isochromatic fringe

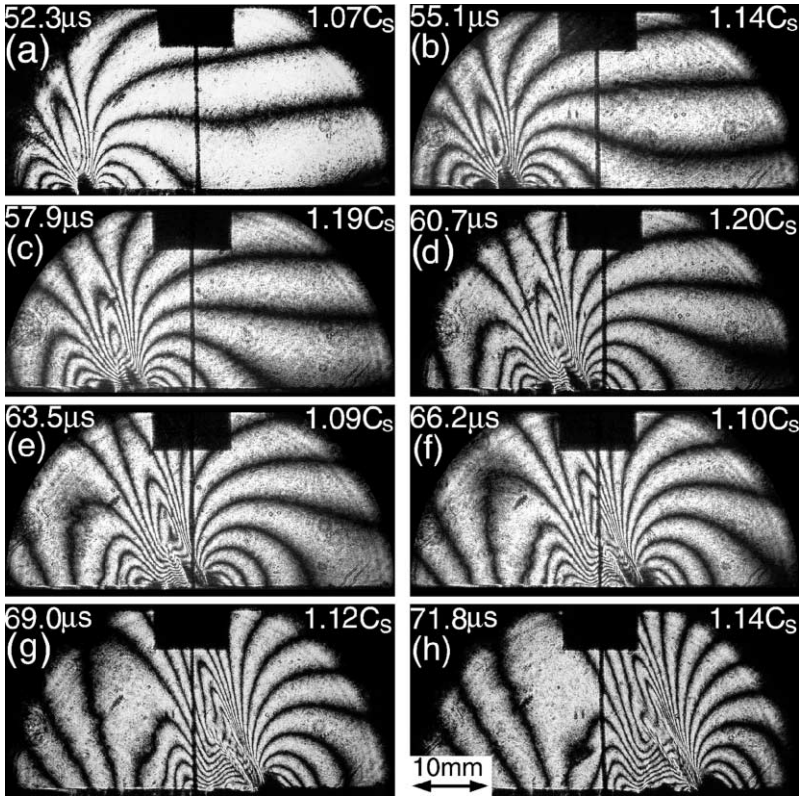

Fig. 5. Isochromatic fringe pattern around an intersonic crack propagating along a Homalite/aluminum interface. Impact speed, $V = 9.9$ m/s. The semicircular field of view of 50 mm diameter is centered on the interface 37 mm ahead of the initial precrack tip. Multiple Mach waves emanating from the crack tip region are clearly visible.

pattern changes abruptly. The angle ξ, the Mach waves make with the crack faces can be related to the crack speed v through

$$\xi = \sin^{-1}(c_s/v). \tag{1}$$

More than one traveling Mach waves are clearly seen and such an observation allowed Singh and Shukla [27] to verify Lambros and Rosakis's [24] conjecture that an intersonic crack tip propagates with a finite zone of crack face contact behind it. Also in Fig. 5(h) we can see a secondary disturbance trailing the propagating intersonic crack tip, which is later shown to be traveling at c_R of the polymer.

Typical crack length and crack speed histories for two similar and representative experiments varying only in the position of the field of view are shown in Fig. 6. In Expt04 and Expt24, the projectile speed at impact was ≈9.6 m/s and the field of view included the initial precrack tip. In Expt18 and Expt19, the projectile speed at impact was ≈9.9 m/s and the field of view was located further downstream from the initial precrack tip. Fig. 6(a) shows the crack length history for all four experiments. Crack length includes the length of the precrack which was ≈25 mm. Error made in measuring the crack length from recorded isochromatic fringe patterns was of the order of ±0.5 to ±1.0 mm. Error bars are shown on a few data points at the beginning and the end of the data set, however, since they are smaller than the symbol size, they are not clearly visible. The time of impact is considered to be the reference point on the time scale and hence $t = 0$ μs corresponds to the time at which the projectile impacts the specimen. After a few microsecond from the time of initiation, the crack length seems to increase almost linearly with time, indicating

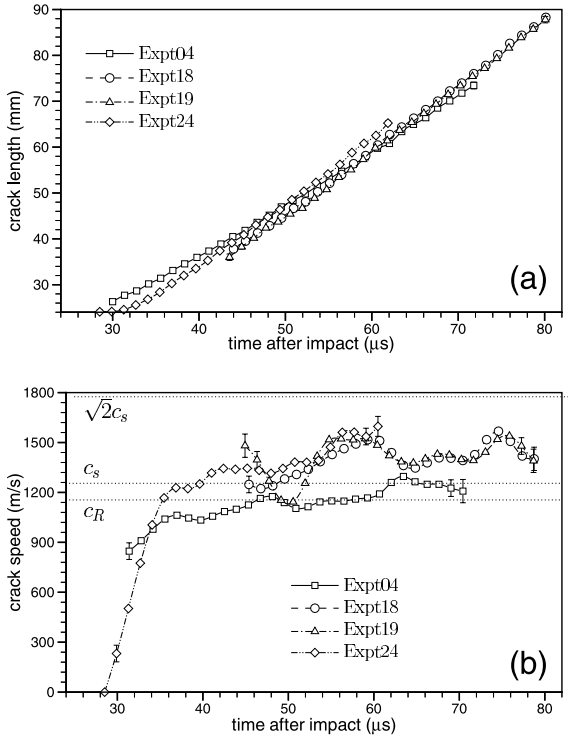

Fig. 6. (a) Time history of crack length. Crack length includes length of the starter notch. (b) Evolution of crack speed v. Expt04 and Expt24 correspond to an impact speed of 9.6 m/s, whereas Expt18 and Expt19 correspond to an impact speed of 9.9 m/s. All the experiments were performed on Homalite/aluminum bimaterial specimens and specimen thickness was 4.8 mm in Expt24 and 6.4 mm in the other three.

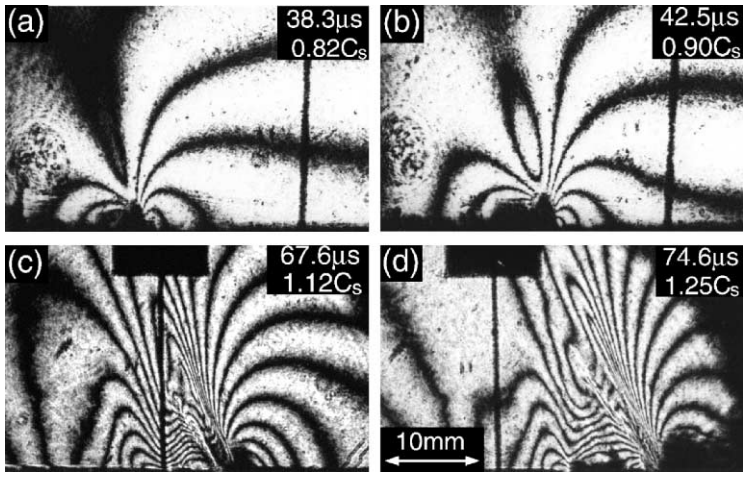

Fig. 7. Comparison of the isochromatic fringe patterns around subsonic and intersonic cracks on a Homalite/aluminum interface. Note the strong Mach wave radiation from the intersonic crack tips.

that the crack is propagating at nearly the same speed. To determine the crack speed, a second order interpolating polynomial was obtained for every three successive points in the crack length history, which is then differentiated with time to give the crack speed for the mid-point. The crack speed history as the interface crack propagates along the Homalite/Al interface is shown in Fig. 6(b) for the same four experiments. From the figure, we see that the interface crack immediately after initiation, accelerates rapidly to speeds higher than c_R of the polymer. In three of the experiments (except Expt04) it is seen that the interface crack becomes intersonic, but seems to propagate at a speed oscillating between c_s and $1.3c_s$. Error in measuring crack speed varied from ± 50 to ± 120 m/s. Error bars are shown on a few points at the beginning and the end of the data set.

Fig. 7 shows a selected set of four isochromatic fringe patterns drawn from two experiments performed under similar conditions. Fig. 7(a) and (b) were taken from Expt04 and Fig. 7(c) and (d) were taken from Expt18. Both these experiments were performed under nominally identical conditions and differences, if any, were discussed in the previous paragraph. The interfacial crack moves from left to right, with the instantaneous crack tip speed and the time elapsed from impact being noted in the top right-hand corner of each frame. These recorded patterns are displayed together in order to demonstrate the dramatic change in the isochromatic fringes, i.e. the nature of the stress field, around the crack tip as it accelerates from subsonic speeds to intersonic speeds. Whereas in the first two images where the crack speeds are $0.82\,c_s$ and $0.90\,c_s$, respectively, the fringes converge smoothly at a distinct point on the interface forming well defined lobes. The fringes in the latter two images, where the crack speed is intersonic, become increasingly compressed and more complex, featuring two distinct shear shock waves emanating from the crack tip and possibly from an end of a well formed contact zone. In the intersonic patterns, we can also clearly distinguish a Rayleigh disturbance trailing behind the crack tip.

5. Subsonic/intersonic transition of a bimaterial interface crack

As mentioned before, the main thrust of the current experimental investigation is to understand the subsonic/intersonic transition of an interfacial crack. To carefully monitor the changes in the stress field in the crack tip region, a magnified view of the isochromatic fringe pattern near the crack tip is shown at

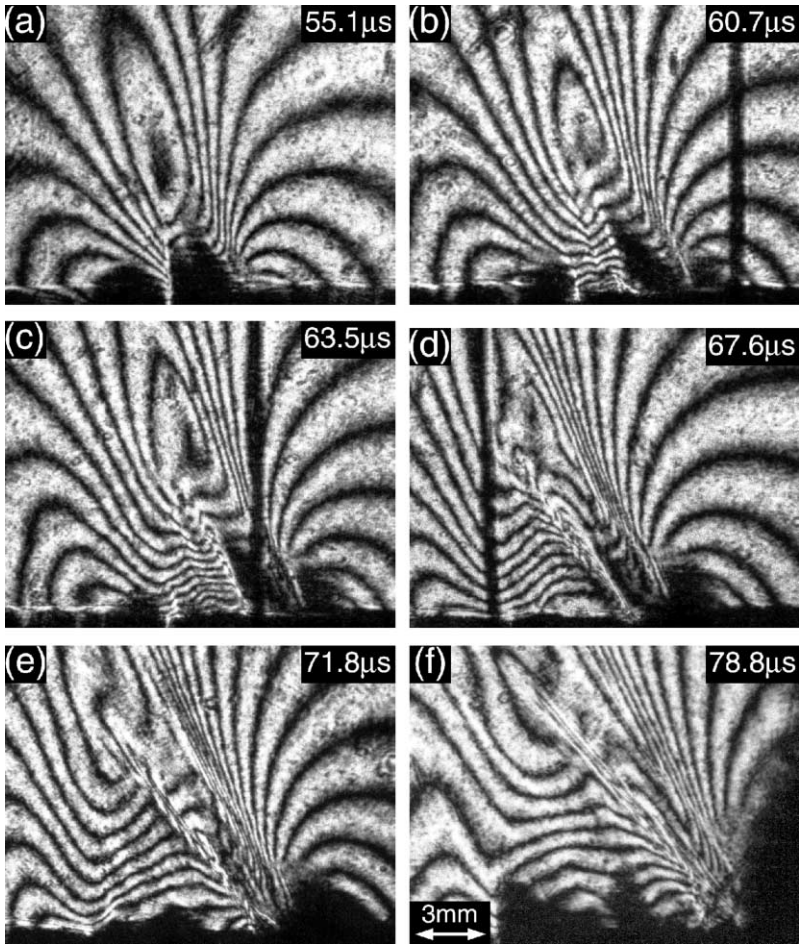

Fig. 8. Crack face contact and multiple Mach wave formation during intersonic crack growth along a Homalite/aluminum interface (Expt18). A magnified view of the area around the crack tip is shown. Impact speed, $V = 9.9$ m/s.

different intervals as it undergoes this transition. All the six magnified views shown in Fig. 8 were borrowed from the experimental records of Expt18 and the crack speed history for that experiment was shown in Fig. 6(b). In all the six views shown, the crack speed is super-Rayleigh (above c_R) and oscillates between c_s and $1.35c_s$. No strong correlation was observed between a particular change in the near-tip stress field and the crack speed, indicating that this subsonic/intersonic transition is a highly transient event, where parameters other than crack speed come into play. In Fig. 8(a), we can identify the crack tip to be located at a point along the interface where the smoothly curving fringes in the front converge on to the interface. Note that the interfacial crack is moving from left to right. A substantial distance behind this point we see an almost vertical Mach wave radiating into the polymer half, across which the isochromatic fringe pattern changes abruptly. We see that such a separation of the front and back lobes of the isochromatic fringe pattern is the first characteristic feature of the subsonic/intersonic transition. If the interfacial crack were propagating at subsonic speeds, both the front and back lobes would meet at a single point, the crack tip [49]. The presence of this near vertical Mach wave can be understood as follows. A moving interfacial crack may be considered to be a moving traction distribution on the polymer surface. It was shown by Freund [50] that such a traction distribution, as it accelerates through the Rayleigh wave speed of the medium, results in a sin-

gularity in surface displacements as well as stresses, which trail the moving load and travel at c_R of the medium. He also showed that this singularity is one-sided, indicating that the stress field on either side of this traveling singularity is not necessarily the same. We believe that such features are indicated by the presence of the vertical Mach wave, on either side of which the nature of stress field is different (isochromatic fringe pattern is different) and moreover seems to indicate that the stress field is singular only behind the vertical Mach wave. It may be fairly conjectured that behind the vertical Mach wave, the crack faces are traction free, however, it is as yet unclear whether the crack faces in front of this Mach wave are in contact or traction free. Also, near-tip solutions for a steady subsonic—super-Rayleigh crack show that the stress fields in front of the tip are no longer singular but pure oscillatory. However, it is doubtful whether such a steady solution is valid during the transition phase, which is likely to be highly transient.

In Fig. 8(b) we see a zone of finite width growing from where the vertical Mach wave was observed before. Because of the higher concentration of isochromatic fringes here, it may be safely conjectured that this zone is a zone of high stresses, most likely due to compressive normal stresses resulting from crack face contact. Hence this zone is likely a crack face contact zone where frictional sliding takes place and ahead of it is a zone of stress field relaxation or what we euphemistically term as a "traction-free zone". This conjecture is different from that put forward by Lambros and Rosakis [24] and Singh and Shukla [27] where it was argued that the crack face contact zone originates right behind the intersonic crack tip. This kind of a detached contact zone is also observed in many other physical phenomena. Schallamach [51] in his quasi-static sliding experiments between rubbers and hard materials, found that displacement along the interface occurs sometimes as macroscopically uniform frictional sliding and sometimes as narrow propagating waves of detachment. The current phenomenon under investigation, where the very compliant polymer is sliding over hard metal at very high slip rates of the order of few m/s, is reminiscent to the one observed by Schallamach. Adams [52] pointed out that if an elastic body is slid against a rigid substrate, dynamic instabilities may occur similar to Schallamach waves, especially in cases where the friction coefficient and Poisson's ratio are quite large. Similar features were also observed in the wrinkle like slip pulse propagation between two dissimilar material interfaces at high slip rates by Andrews and Ben-Zion [4] and by Ranjith and Rice [6]. Detached contact zones were also observed in the dynamic numerical simulations of Breitenfeld and Geubelle [38] and Needleman and Rosakis [39]. At the original position of the vertical Mach wave, we now have a weak Mach wave across which the fringes merely change their slope. Hence Fig. 8(b) shows a triple Mach wave structure, one emanating from the crack tip and the other two emanating from the front and rear ends of the contact zone, with the weak one corresponding to the rear end of the contact zone.

At later times we see that the size of the contact zone diminishes, with the weak Mach wave moving towards the one emanating from the front end of the contact zone, shrinking the contact zone size to zero (Fig. 8(c)). Indeed in Fig. 8(d), we find that the contact zone almost vanishes as the Rayleigh singularity trails further behind the intersonic crack tip. Here the contact appears to be almost infinitesimal (single point) from the fact that the distance between the second and the third Mach waves is almost negligible and a two Mach wave structure is recovered. As the Rayleigh singularity trails further behind, we subsequently find that the size of the "traction-free zone" also diminishes (see Fig. 8(e)) and eventually vanishes completely (see Fig. 8(f)). The fact that the surviving infinitesimal (point) contact zone catches up with the crack tip can also be seen from the relatively steep inclination of the second Mach wave. Eventually, we find that the intersonic crack emerges traction free in Fig. 8(f) where the Rayleigh singularity is trailing a sufficient distance behind the intersonic crack tip and as the crack tip speed steadily approaches $\sqrt{2}c_s$.

However, these features of the subsonic/intersonic transition of an interfacial crack do not appear to be universal. In another experiment, Expt19, which was also discussed before, and is nominally identical to Expt18, the essential end feature where the intersonic crack emerges traction free is not observed. Fig. 9 shows a sequence of six magnified views of the crack tip region as the interface crack in Expt19 undergoes the subsonic/intersonic transition. The initial features like the formation of point contact (see Fig. 9(a)),

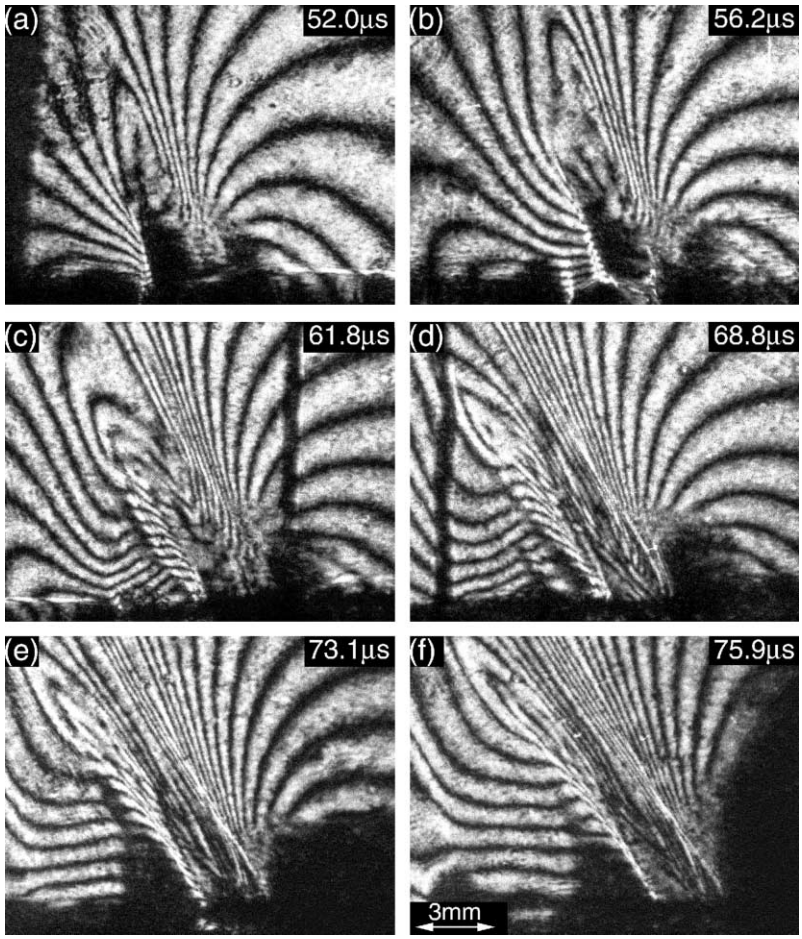

Fig. 9. Crack face contact and multiple Mach wave formation during intersonic crack growth along a Homalite/aluminum interface (Expt19). A magnified view of the area around the crack tip is shown. Impact speed, $V = 9.9$ m/s.

growth of contact region (see Fig. 9(b)), diminishing of the contact zone to an infinitesimal size (single point) (Fig. 9(c)–(e)) were all observed, as in Expt18. However, unlike in the case of Expt18, even as the Rayleigh singularity trails sufficient distance away from the intersonic crack tip, the infinitesimal contact zone seems to remain at a constant distance behind the intersonic crack tip, as indicated by the two parallel Mach waves emanating from these two features (see Fig. 9(f)). Within our experimental field of view, no emergence of a completely traction-free intersonic crack was observed, as was the case in Expt18.

The same orderly change in the nature of the isochromatic fringe pattern in the crack tip region, as was observed in Expt18, was found to be highly repeatable and was observed in at least five other similar experiments. However, even without any substantial differences as to the specimen dimensions, properties of the interface and the loading conditions, in a particular experiment (Expt19), the change in the nature of the isochromatic fringe pattern during subsonic/intersonic transition was found to be slightly different. Hence the subsonic/intersonic transition examined above does appear to depend on additional parameters apart from the mere fact that the crack speed accelerates through the Rayleigh and shear wave speeds. As observed by Schallamach in his experiments, it might depend substantially on the interface characteristics.

Figs. 10 and 11 show a set of four enlarged views of the isochromatic fringe pattern at different times around the tip of an intersonic crack propagating on a Homalite/steel interface. The dimension of the rectangular field of view is $\approx 20 \times 15$ mm. The projectile impact speed was $V = 9.7$ m/s, which is very close to V for Expt18 and Expt19, the results of which were discussed before. These records were made using a high speed digital camera (Cordin model 220) with a much smaller optical path length as compared to the high speed film camera described in Section 2. However, the high speed digital camera records a mere eight frames during the dynamic event and hence parameters like time after impact and crack speed cannot be estimated accurately for each frame. However, for intersonic crack growth, the inclination of the Mach angle ξ emanating from the crack tip uniquely identifies the crack tip speed (see (1)). Crack tip speed thus obtained is shown on each of the four frames in Figs. 10 and 11. Also, an area around the crack tip bounded by the rectangle drawn is shown as an inset to the top right of each frame. Except for Fig. 10(a), where the inset shown is magnified, the rest of the insets are the same size as the bounded rectangles.

In Fig. 10(a), we can see that the interface crack has just attained intersonic speed, from the fact that the Mach waves emanating from the crack tip region have radiated only a short distance into the polymer. From the inset of this frame, we can clearly see the Mach wave emanating from the crack tip ahead of which the fringes are smoothly curved and behind which the fringes close to the interface are almost parallel to it. However, this behavior of the isochromatic fringes behind the crack tip changes abruptly within a short distance of 2 mm, where yet another Mach wave seems to be emitted from the ruptured interface. We interpret this zone between the two Mach waves as a traction-free zone, where there is a relative sliding of the polymer and metal surfaces with an accompanied relaxation of the normal compressive stress, after the

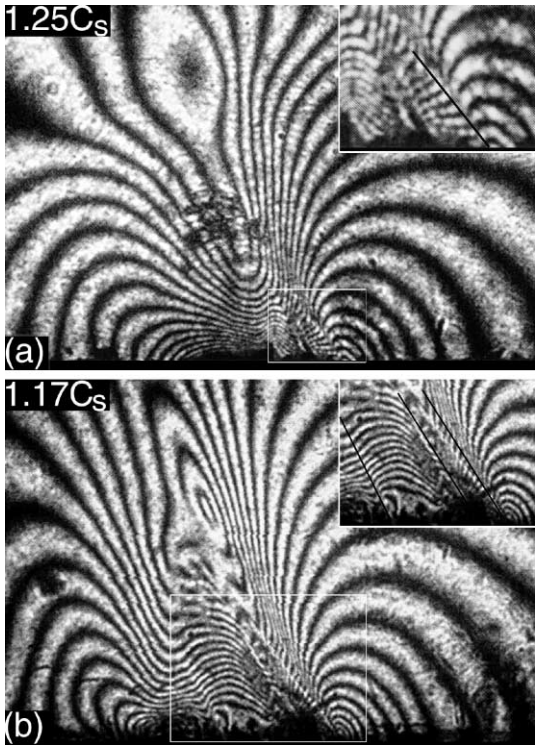

Fig. 10. (a) Isochromatic fringe pattern around an intersonic crack on a Homalite/steel interface—I. Three Mach waves can be seen clearly in (b) indicated by the three black lines (inset). Impact speed, $V = 9.7$ m/s.

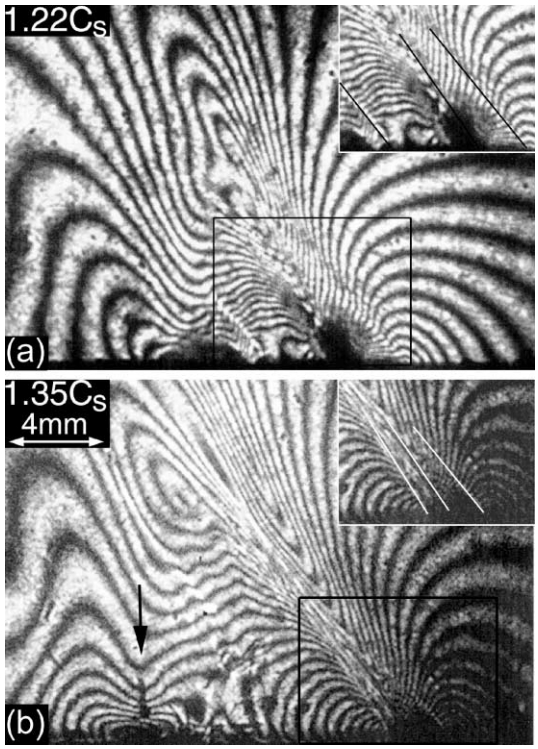

Fig. 11. Isochromatic fringe pattern around an intersonic crack on a Homalite/steel interface—II. (a) Shows the three Mach wave structure and (b) shows the fringe pattern unaffected by the Rayleigh singularity.

interface is broken by the moving intersonic crack tip. Behind the second Mach wave, we can identify yet another region, approximately 2 mm long where we conjecture that the crack faces are under strong normal compressive stress and sliding with frictional contact takes place here. As the interface crack propagates further, we can clearly distinguish the three Mach waves emanating from the crack tip region as they have radiated over a sufficient distance into the polymer half (see Fig. 10(b)). The two zones—traction-free zone behind the crack tip (or zone of low normal compression) and the crack face frictional contact zone can be clearly identified. All the three Mach waves seen are inclined at almost the same angle of $\approx 59°$, showing that these features are moving at about the same speed. However, as compared to Fig. 10(a), the length of the frictional contact zone has increased substantially to about 3.8 mm. Such an initial growth of contact region as the intersonic crack propagates further along the interface was also seen in Figs. 8 and 9.

Two more frames showing the isochromatic fringe pattern around the crack tip at later times are shown in Fig. 11(a) and (b). The three Mach waves and the two distinct zones in the crack tip region—traction-free zone and the frictional contact zone are very clearly identifiable in these figures. Fig. 11(a) is similar to Fig. 10(b) with length of the traction-free zone being approximately equal to 2 mm and the length of the frictional contact zone being approximately equal to 3.8 mm. The two Mach waves emanating from the crack tip and the front end of the contact zone are almost parallel inclined at an angle of $\approx 55°$ to the interface, whereas that emanating from the trailing end of the contact zone is inclined slightly steeper at almost 60° to the interface. This steeper inclination of the Mach wave emanating from the trailing end of the frictional contact zone seems to indicate that the contact zone might reduce in size, which is exactly what is seen in Fig. 11(b). Here the contact zone seems to diminish in size and eventually vanish to a single point. However, the length of the traction-free zone has remained almost the same, indicating that inter-

sonic crack growth along the Homalite/steel interface seems to propagate further with a finite sized traction-free zone and a point sized contact behind the tip. This observation is akin to that found for intersonic crack growth along a Homalite/aluminum interface in Fig. 9, i.e., for Expt19. The Rayleigh singularity is trailing sufficiently far behind the crack tip and can be clearly identified in Fig. 11(b), as the point where the fringes bend in a V-shape almost 13 mm behind the crack tip. By this time, i.e., with a sufficient separation between the intersonic crack tip and the trailing Rayleigh singularity, the intersonic crack was found to emerge with traction-free crack faces in most experiments (see Fig. 8). However, as seen in Figs. 9 and 11, it may not always be the case and the intersonic interfacial crack seems to propagate ahead with still a finite sized traction-free zone and a infinitesimal contact zone behind the tip. Owing to the limited size of the field of view and limited extent of the interface, further events could not be captured to see if there is indeed a universal character to the above observations. It is very much desirable to focus future experiments on intersonic crack growth along a bimaterial interface to resolve this ambiguity, as far as the subsonic/intersonic transition event is concerned. If indeed different phenomena are possible, it would be desirable to find out the relevant parameters that govern the emergence of one phenomenon over the other.

We discussed the subsonic/intersonic transition event quite extensively above, carefully examining the crack tip region during the transition in three different experiments, two of which involved a Homalite/Al interface and one of which involved a Homalite/steel interface. All these experiments were performed under nominally identical conditions—similar specimen dimensions and preparation methods, same projectile impact speeds, same initial crack lengths, etc. We identified that the features observed during the transition event are similar, however, the question whether the intersonic interfacial crack eventually emerges traction free or not was not completely resolved. Most of the experimental results point to the former case, though a certain number of experiments point to the latter. More study is required to resolve the issue. However, the general features associated with the subsonic/intersonic transition of an interfacial crack on a polymer/metal interface are laid out in an illustration shown in Fig. 12. It shows our conjecture of the different events happening during the transition and they are described in five sketches of the crack faces (A)–(E) in Fig. 12. The origin of the crack tip coordinates (η_1, η_2) indicates the location of the crack tip. In (A), the crack is propagating subsonically and the crack faces are essentially traction free. In (B) as the crack exceeds c_R of the polymer, a one sided singularity in the stress field is generated as indicated by the almost vertical Mach wave emanating from the point where the interfacial crack exceeded c_R. The crack face of the polymer half appears to be still in contact with the metal half here, under strong normal compression undergoing frictional sliding. The inclined Mach wave emanating from the crack tip indicates that it is moving at intersonic speeds and away from the Rayleigh singularity. In between these two points, we conjecture that the crack faces are traction free or at least under a relaxed normal compression. (C) shows that as the intersonic interfacial crack moves further away from the Rayleigh singularity, the size of the contact zone grows and the three Mach waves emanating from the crack tip, the front and trailing ends of the contact zone are almost parallel to each other indicating that they are all moving at the same speed (see Figs. 10(b) and 11(a)). At still later times, as the intersonic crack tip moves further away from the Rayleigh singularity, the contact zone size diminishes, as shown in (D) with only two Mach waves emanating, one from the crack tip and the other from the infinitesimal-sized contact zone. In some experiments, this event was found to go on until the crack tip ran out of the field of view. However, in most experiments it was found that as the Rayleigh singularity trails sufficiently far from the tip, the contact zone moves rapidly into the crack tip, vanishes and the crack faces were found to emerge traction free as shown in (E).

Fig. 13 shows an enlarged view of the sketch (C) of Fig. 12. Here the intersonic bimaterial interface crack is propagating with a finite traction-free zone behind the tip, followed by a finite zone of crack face frictional contact. The location of the Rayleigh singularity is also shown. The lengths of the traction-free zone and the frictional contact zones are termed l_1 and l_2 respectively. Also, the inclination to the interface, of the Mach waves emanating from the crack tip and the front end of the contact zone are termed α and β respectively. The sketch essentially introduces the nomenclature adopted from now on, and in the next two

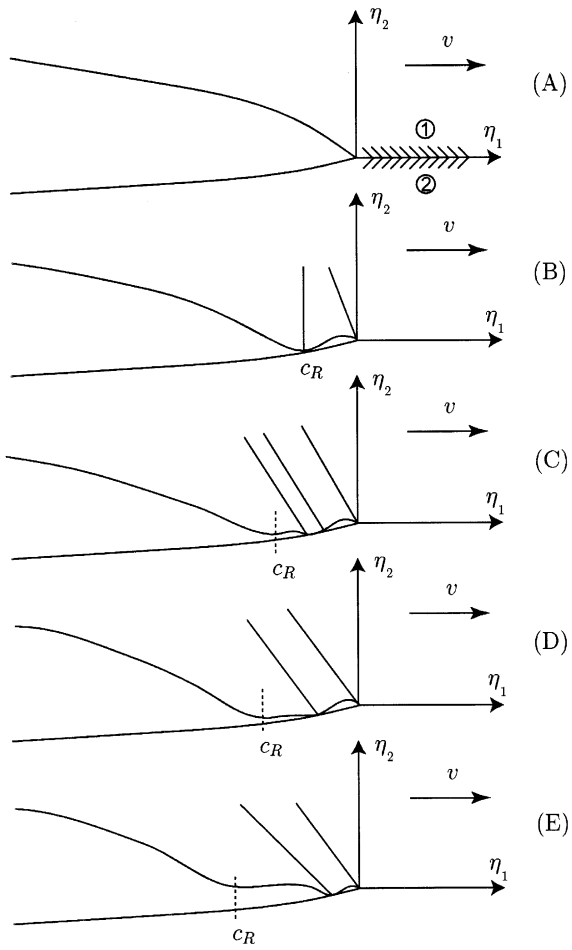

Fig. 12. An illustration summarizing empirical interpretations regarding the formation of crack face traction free and contact zones during acceleration of an interfacial crack from subsonic to intersonic speeds.

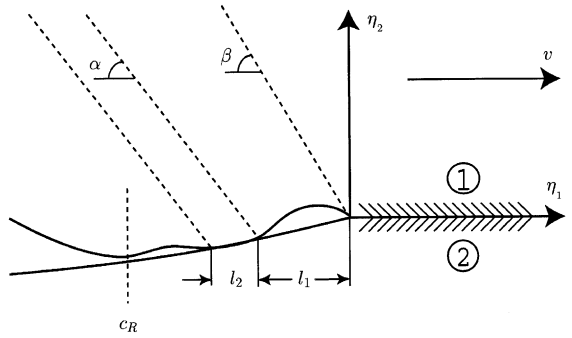

Fig. 13. An illustration showing the various parameters associated with an intersonic bimaterial interface crack with finite crack face traction free and frictional contact zones.

figures the variation of some of these parameters as the intersonic crack propagates along the bimaterial interface is shown.

6. Mach angles and zone lengths

Fig. 14(a) shows the variation of the Mach wave angles α and β (see Fig. 13) with time as the intersonic crack propagates along the bimaterial interface. Experimental records of isochromatic fringe patterns from two experiments—Expt18 and Expt19 (the same experiments discussed before), which were performed under nominally identical conditions, were analyzed to obtain the time history of the Mach wave angles, α and β. As seen from Fig. 14(a), β for Expt18 and both α and β for Expt19 range between 60° and 70°. However, α for Expt18 starts initially around 80° and falls almost to 50° by the time crack exceeds the field of view. These observations can be interpreted easily as follows. In Expt18, it was found that the Mach wave emanating from the front of the contact zone was almost vertical in the beginning, which eventually catches up with the crack tip by the time the crack runs out of the field of view. Hence the inclination of the Mach wave emanating from the contact zone becomes smaller and smaller indicating that it is catching up with the intersonic crack tip. However, in the case of Expt19, the two Mach waves from the crack tip and the front end of the contact zone were always parallel as can be seen in Fig. 14(a).

Fig. 14(b) shows the variation of crack speed with time as obtained from the Mach angle history given in Fig. 14(a) and by using (1). It can be seen that the crack tip in Expt18 is traveling at a near constant speed

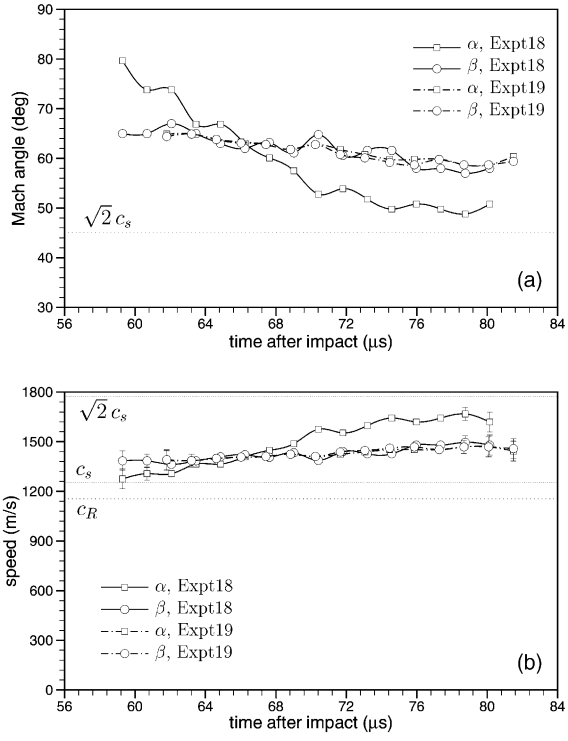

Fig. 14. (a) Time history of Mach angle. β is the inclination of the Mach wave emanating from the crack tip and α is the inclination of the Mach wave emanating from the front end of the contact zone. (b) Speed from Mach angle histories above. Expt18 and Expt19 are the same as those in Fig. 6.

increasing only slightly from around $1.05c_s$–$1.25c_s$. In Expt19, both the crack tip as well as the front end of the contact zone move at the same speed ranging between the same limits above. Hence the observation that in Expt19, where the detached contact zone was always found at the same distance behind the crack tip. However, in Expt18, where the detached contact zone accelerates, catches up with the crack tip and vanishes, the crack speed associated with the front end of the contact zone was found to increase substantially and eventually exceed that of the crack tip.

Fig. 15(a) shows the variation of the length of the traction-free zone (l_1) and the frictional contact zone (l_2) for the same two experiments—Expt18 and Expt19. In Expt18, it was found that the contact zone starts point sized, grows to a finite size and eventually reduces back to infinitesimal size. Similar behavior was also found in Expt19. This is in agreement with the illustration of our conjecture regarding subsonic/intersonic transition shown in Fig. 12. The length of the traction-free zone (l_1) in Expt18 after being constant for a while, eventually shows a decrease essentially agreeing with the earlier observation that the intersonic crack eventually emerges traction free. However, in Expt19, no such traction-free crack emerges and hence the length of the traction-free zone was found to be almost constant as the intersonic crack travels through the field of view. Also, l_1 was found to be utmost of the order of 3 mm and l_2 was found to be utmost of the order of 2 mm. Hence these zones are finite sized, unlike in the case of subsonic interfacial crack growth, where the crack face contact zone remains infinitesimally small, except for speeds very close to c_R.

Fig. 15(b) shows the variation of the speed of the Rayleigh singularity with time. Data is taken from the same two experiments—Expt18 and Expt19. Data essentially agrees with our assumption as to the feature in the isochromatic fringe pattern identifying the Rayleigh singularity, as it is found to propagate at a constant speed through out the field of view, very close to c_R of Homalite. The presence of this Rayleigh

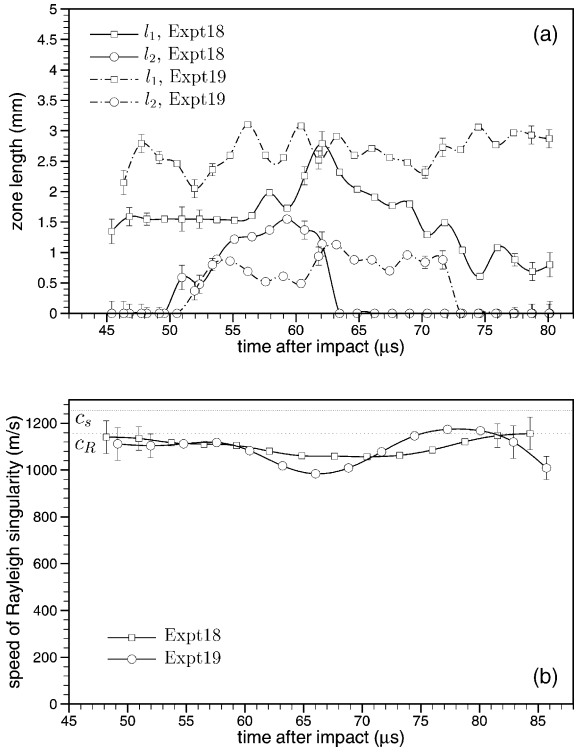

Fig. 15. Intersonic crack growth along a Homalite/aluminum interface. (a) Time history of crack face traction free and frictional contact zone lengths. (b) Speed of Rayleigh singularity. Expt18 and Expt19 are the same as those in Fig. 6.

singularity close to the intersonic crack tip is the prime reason for the evolution of the multiple features observed during the subsonic/intersonic transition of a bimaterial interface crack.

7. Effect of geometry and impact speed on the attainment of intersonic crack speeds on a bimaterial interface

Further experiments on intersonic crack growth along a polymer/metal interface were performed with a different specimen geometry to ascertain the effect of finiteness of the specimen dimensions on the propagation behavior of the intersonic crack. An elongated specimen geometry shown in Fig. 16 was adopted and specimens with PMMA and steel as the two constituents were prepared following essentially the same procedure as given in Section 2. Because of the smaller height of the specimen compared to the specimen geometry shown in Fig. 1, reflected waves from the free surface impinge back onto the propagating crack tip possibly resulting in an alteration of the propagation behavior of the intersonic interfacial crack. Since PMMA is not birefringent, CGS interferometry was used to record the stress field information around the propagating crack tip.

Fig. 17 shows two selected CGS interferograms around the tip of an intersonic crack propagating on a PMMA/steel interface. The specimen was impacted by a cylindrical steel projectile at a speed, $V = 19.2$ m/s, and the semicircular field of view of 50 mm diameter was centered on the interface a distance of 15 mm ahead of the precrack tip. For subsonic interfacial crack propagation, the CGS fringe pattern consists of two smoothly curving lobes which converge to a single point on the interface, the crack tip. As the interfacial crack attains intersonic speeds, the front lobe is no longer smooth and round, but develops a kink, where the fringes suddenly dip towards the interface (see Fig. 17(a)). This feature is caused by the fact that the point where the two lobes meet is no longer the actual crack tip, but is merely the location of the Rayleigh singularity. The intersonic crack tip has slid forward and the Mach wave radiating from here produces a increased stress gradient, which is reflected as an increase in the fringe order along this line, which eventually manifests itself as a sudden bending of the CGS fringes towards the interface (see Fig. 17(b)). Note that CGS interferometry is insensitive to shear Mach waves and hence they are not seen explicitly. Thus, while analyzing CGS interferograms for the speed of an intersonic interfacial crack, one has to be very careful in identifying the location of the crack tip. Eventually, as the Rayleigh singularity trails sufficiently far from the crack tip, the crack tip stress singularity takes over, as identified by the fact that the kink in the front lobe eventually dips to the interface. It may be noted here that due to the finite height of the specimen, reflected waves from the top surface, continuously interfere with the crack tip fields resulting in fringes that have a very jagged structure.

Crack speed history for two similar and representative experiments varying in the position of the field of view and projectile impact speed are shown in Fig. 18. In Expt31, the projectile speed at impact was ≈19.2 m/s, and in Expt32, the projectile impact speed was ≈14.5 m/s. Both these experiments involve elongated PMMA/steel specimens and stress field information around the propagating crack tip was recorded using

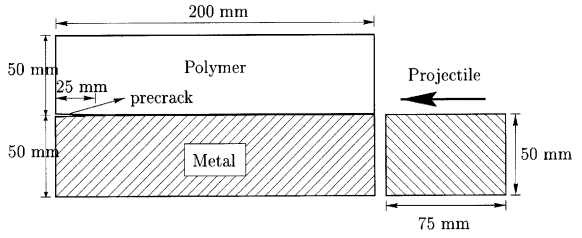

Fig. 16. Elongated bimaterial specimen with a precrack subjected to impact shear loading.

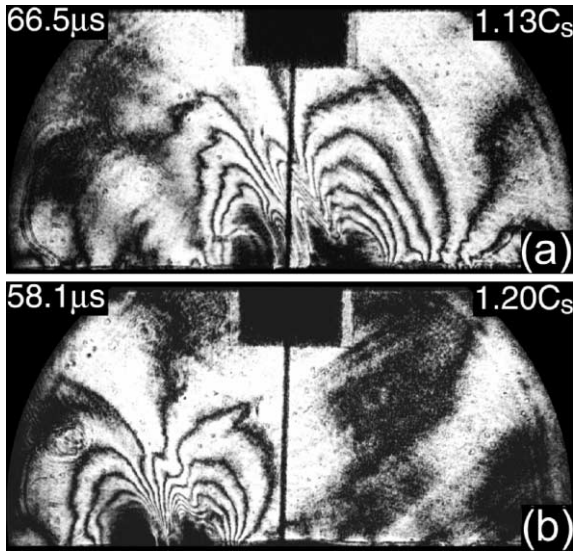

Fig. 17. CGS fringe pattern around an intersonic crack propagating along a PMMA/steel interface loaded under impact configuration (B). Impact speed, $V = 19.2$ m/s. The semicircular field of view of 50 mm diameter is centered on the interface 15 mm ahead of the initial precrack tip.

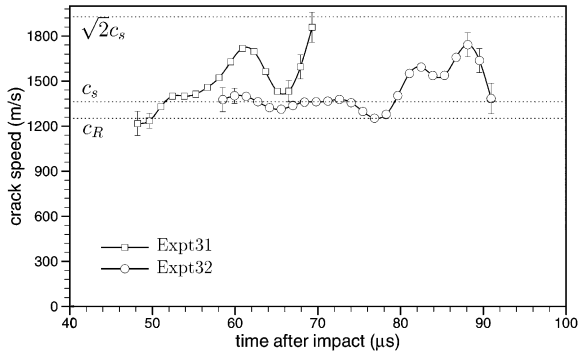

Fig. 18. Intersonic crack growth along a PMMA/steel interface. Evolution of crack speed v. In Exp31, projectile impact speed, $V = 19.2$ m/s and in Exp32, $V = 14.5$ m/s.

CGS interferometry. The field of view in Expt32 was located further downstream from the initial precrack tip. Again, the time of impact is considered to be the reference point on the time scale and hence $t = 0$ μs corresponds to the time at which the projectile impacts the specimen. From the figure, we see that the interface crack propagates at a speed close to c_s as soon as it enters the field of view, but eventually accelerates to higher intersonic speeds. However, it was always found that the crack speed remains below $\sqrt{2}c_s$. The importance of the curious speed $\sqrt{2}c_s$ with regard to intersonic interfacial crack propagation (with high wave speed mismatch) was discussed in [28,35]. Note that the projectile impact speed V in both the experiments shown in Fig. 18 is substantially higher than that seen in Fig. 6(b), and hence the observed higher crack speeds. Also the finite height of the specimen with resulting in wave reflections towards the crack tip might be responsible for the increased fluctuations in crack speed. Error in measuring crack speed varied from ±50 to ±160 m/s. Error bars are shown on a few points at the beginning and the end of the data set.

To determine the effect of impact speed on the attainment of intersonic crack speeds on a bimaterial interface, data is drawn from several experiments which were performed under nominally identical conditions, except for the impact speed. All these experiments involve PMMA/steel bimaterial specimens with an edge precrack and their dimensions are the same as those given in Fig. 1 and were prepared following the procedures described in Section 2. All the specimens were loaded by impact, either by a cylindrical steel projectile fired from a high speed gas gun or by a drop weight tower under the loading configuration (B) as defined in Fig. 1. Fig. 19 shows the variation of interfacial crack speed with time for five such experiments, in two of which the bimaterial specimens were loaded at low impact speeds, 3 and 4 m/s respectively using a drop weight tower and in the rest three the specimens were loaded at high impact speeds, 17, 20 and 28 m/s respectively. Crack speed data was obtained from crack length history by the same procedure mentioned previously. As seen from the figure, for an impact speed of 3 m/s, the crack initiates at almost 90 μs after impact, accelerates slowly and always remains subsonic. At a slightly higher impact speed of 4 m/s, the precrack is observed to initiate earlier, around 60 μs after impact, accelerates faster, but still remains subsonic. However, in all the gas gun loaded experiments involving high impact speeds, the precrack seems to initiate almost at the same time, around 30 μs after impact, then accelerates rapidly through c_R and c_s of the polymer and becomes intersonic. It oscillates between c_s and $\sqrt{2}c_s$ for a while and remains within this range for an impact speed of 17 m/s. For higher impact speeds at 20 and 28 m/s the intersonic crack is suddenly found to accelerate yet again to speeds above $\sqrt{2}c_s$ of the polymer and in the last case, almost seems to exceed c_l of the polymer thus becoming supersonic with respect to it. However, it is interesting to note that in all the experiments where the crack has attained intersonic speeds, the precrack seems to initiate at exactly 30 μs after impact. To understand this intriguing phenomenon, we must look at the various features associated with the wave propagation from the impact site.

Fig. 20 shows roughly the wavefronts associated with the stress wave propagation from the impact site. The primary longitudinal wave emanating from the impact site traverses through the metal half, reflects from the opposite free end and impinges back on the crack tip and loads it in intense shear around 30 μs after impact. Note that the loading history at the initial crack tip is primarily due to waves traveling in the metal half. The experimentally measured initiation time of 30 μs (see Fig. 19) after impact correlates very well with the time it takes a dilatational compressive wave in steel to travel the height of the specimen, reflect off the bottom surface as a tensile wave and reach the initial crack tip. Hence in all high speed impact experiments, at initiation the precrack is under highly shear dominated conditions. This conclusion

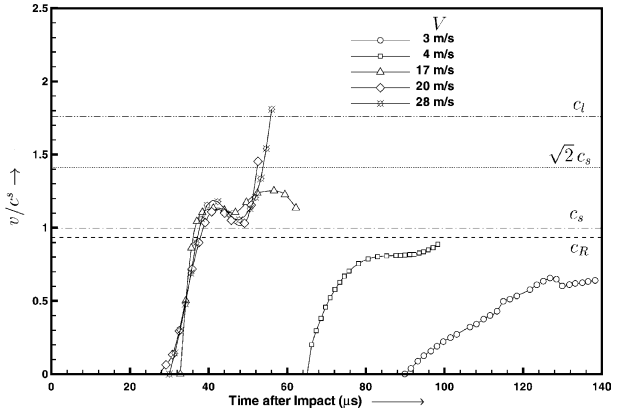

Fig. 19. Crack growth along a PMMA/steel interface—Effect of impact speed on crack speed history. At an impact speed higher than a threshold value, the interface crack attains intersonic speeds. V is the projectile impact speed and v is the interface crack speed.

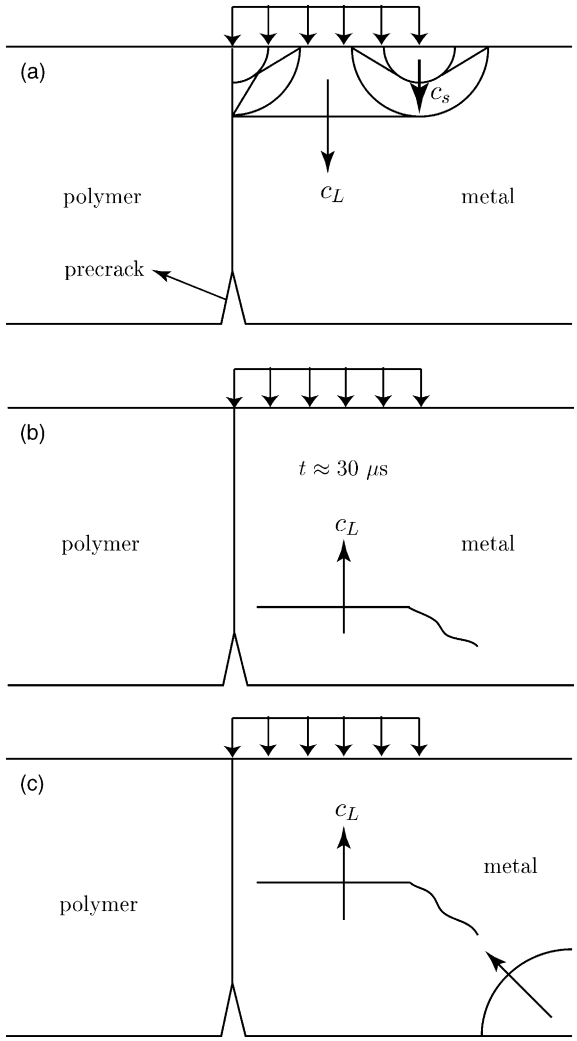

Fig. 20. An illustration showing roughly the propagation of loading waves in the metal half of the bimaterial specimen after impact. Interfacial cracks that attain intersonic speeds are highly shear dominated at initiation.

is also supported by Lambros and Rosakis [20] who showed that subsonic crack growth achieved through gas gun experiments is predominantly shear dominated. The initiated shear crack under such circumstances is always found to attain intersonic speeds. In low impact speed (<5 m/s) experiments, the stress field around the crack tip at 30 μs (when the dilatational wave in steel arrives at the crack tip after rebounding from the bottom surface) is shear dominated, but did not have a high enough magnitude to initiate the crack. Hence it waits until the unloading wave from the lower right hand corner of the steel side reached the crack tip, some 70–80 μs after impact and loads the tip in an opening mode. Now, a lower magnitude of the stress field is enough to initiate the crack because a substantial opening component is provided. In such a case, it was found that the interfacial crack always remains subsonic. Hence, it appears that one of the conditions under which a loaded precrack becomes intersonic is to be initiated under intense shear.

8. Intersonic crack growth on a bimaterial interface under loading configuration (C)

It was mentioned apriori, that under loading configuration (C), the edge precrack on a bimaterial interface initiated and propagated at intersonic speeds along the interface. Fig. 21 shows a sequence of four isochromatic fringe patterns depicting such an event. Here an edge precrack, 25 mm long, on a Homalite/aluminum interface was loaded by projectile impact under loading configuration (C). The projectile impact speed, V was 20.7 m/s and the semicircular field of view of 50 mm diameter was centered on the interface 45 mm ahead of the initial precrack tip. Again, we see that the interface crack attains intersonic speeds almost immediately after initiation. However, the shape of the fringe pattern around the intersonic interfacial crack tip, differs substantially from that achieved under loading configuration (B). The fringe pattern appears lot more squeezed horizontally and the crack tip fields appear to be dominant over a shorter region, both in front and behind the propagating crack tip. This difference in the shape of the isochromatic fringe pattern (and thus the near-tip stress field) around the intersonic interfacial crack tip achieved from two different loading configurations (B) and (C) can be explained on two counts. First, with the loading configuration (C), the interfacial crack initiates and propagates with the initial loading pulse itself, which is still very strong (not enough time for geometric attenuation) as seen from the number of fringes due to the loading pulse in front of the crack tip. Also the stress induced due to the loading pulse substantially affects the crack tip stress field (primarily with regard to the direct stress parallel to the interface), thus resulting in the squeezing of the fringe pattern both in front and behind the crack tip. Second, the nature of loading is such that the precrack tip is subjected to a strong shearing component, but also to a compressive opening component. This results in enhanced crack face contact, and the entire rupture occurs primarily in shear. This is unlike the scenario from loading configuration (B) where the loading is such as to slightly open up the crack as it propagates, rather than forcing it to close. Indeed, in that case we saw the crack propagate with a finite traction-free zone behind the tip and any crack face frictional contact was primarily due to the presence of Rayleigh singularity. However, in the loading configuration (C), the crack face frictional contact is aided not only by the presence of a Rayleigh singularity, but also due to the nature of loading itself. Hence, with this loading configuration, the crack face frictional contact zone starts much closer to the intersonic crack tip, as compared to that in loading configuration (B). As the intersonic crack propagates

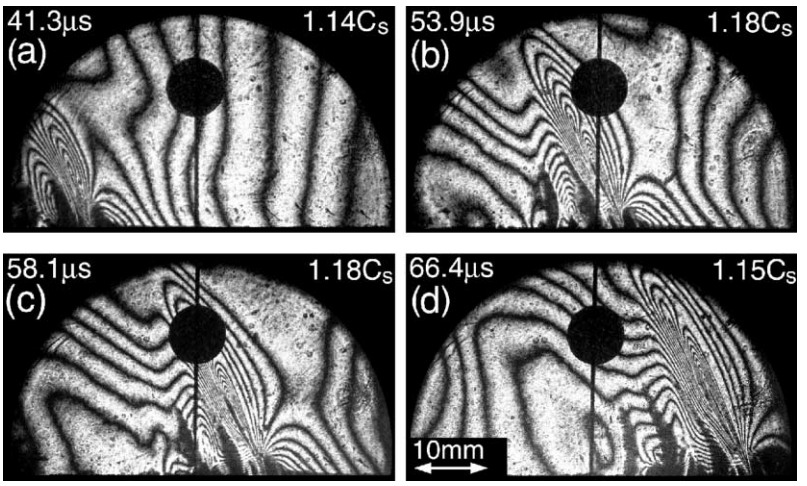

Fig. 21. Isochromatic fringe pattern around an intersonic crack propagating along a Homalite/aluminum interface loaded under impact configuration (C). Projectile impact speed, $V = 20.7$ m/s. The semicircular field of view of 50 mm diameter is centered on the interface 45 mm ahead of the initial precrack tip.

along the interface, no dramatic changes in the isochromatic fringe pattern near the crack tip are visible, indicating that the intersonic crack propagates with an infinitesimal traction-free zone and a finite crack frictional contact zone behind it, throughout the field of view. The presence of an infinitesimal traction-free zone may be conjectured from the presence of two distinct fringe lobes, a bigger lobe enveloping a smaller lobe, behind the crack tip (see Fig. 21(c) and (d)). Also, from Fig. 21(d) we can see the Rayleigh singularity separated a finite distance from the intersonic crack tip, and we observe a series of fringes parallel to the interface joining these two features. These fringes are similar to those observed in the isochromatic fringe patterns obtained with loading configuration (B) within the frictional contact zone. Hence the essential features of the subsonic/intersonic transition of an interface crack is strongly dependent on the "mixity" of the applied dynamic loading.

Typical crack length and crack speed histories obtained from two different experiments, both involving interfacial crack initiation and propagation from an edge precrack loaded under configuration (C) are shown in Fig. 22. In Expt40, the specimen thickness was 4.8 mm, whereas in Expt42, the specimen thickness was 6.4 mm. However, the projectile impact speed V in both experiments was the same at $\approx$20.7 m/s. As seen from Fig. 22(a), the crack length of the interfacial crack increases almost linearly with time as it propagates through the entire field of view. Fig. 22(a) gives the crack speed history obtained by successive three point parabolic fit to the length history and its differentiation to give the crack speed for the mid point. The crack speed history, thus obtained, is shown in Fig. 22(b) for both these experiments. It can be seen that the crack speed remains fairly constant, oscillating between c_s and $1.3c_s$. Thus it appears that specimen thickness does not play much of a role in the propagation behavior of the interface crack. Also the

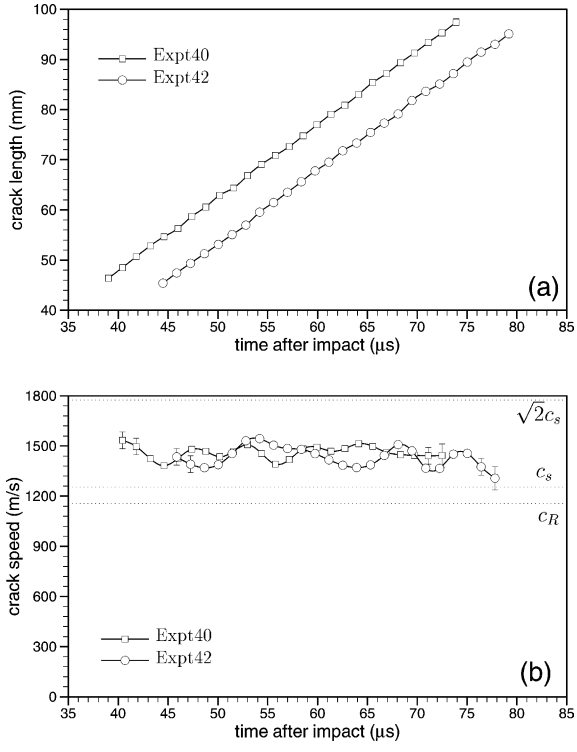

Fig. 22. Intersonic crack growth along a Homalite/aluminum interface loaded under impact configuration (C). (a) Time history of crack length. Crack length includes length of the precrack. (b) Evolution of crack speed v. In both Expt40 and Expt42 the projectile impact speed, $V = 20.7$ m/s. However, specimen thickness in Expt40 was 4.8 mm and in Expt42 it was 6.4 mm.

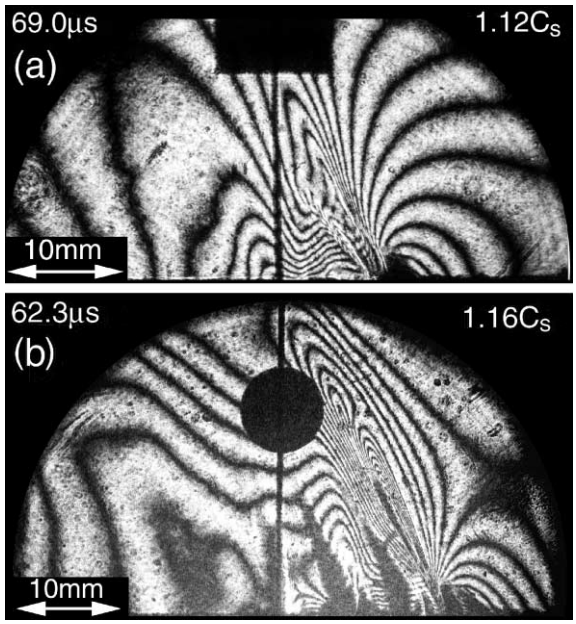

Fig. 23. Intersonic crack growth on a Homalite/aluminum interface. (a) Isochromatic fringe pattern resulting from loading configuration (B). (b) Isochromatic fringe pattern resulting from loading configuration (C).

propagation behavior was similar to that obtained with loading configuration (B), though at almost half the impact speed as was used in these experiments. However, this near constant speed interfacial crack growth between c_s and $1.3c_s$ appears to be some kind of a universal feature for certain ranges of interface strengths and intensities of applied load. As such, it may be reflected in the nature of the intersonic interfacial crack tip fields.

Fig. 23 compares two isochromatic fringe patterns around an intersonic crack propagating along a Homalite/aluminum interface at approximately the same crack speed, but differing in the loading configuration leading to the initiation of these cracks. In Fig. 23(a), the interfacial crack was initiated from an edge precrack under loading configuration (B), where as in Fig. 23(b), the interfacial crack was initiated from an edge precrack under loading configuration (C). The fringe pattern around the crack tip in both these cases shows a marked contrast. In Fig. 23(a), we have an intersonic crack with smoothly curved fringes in front of the crack tip, a sharp Mach wave radiating from the tip and a second Mach wave, again very sharp, radiating from the interface $\approx$2 mm behind the crack tip. As was conjectured before, the crack here is propagating with a finite traction-free zone behind the tip followed by an infinitesimal frictional contact zone. The Rayleigh singularity trailing behind is also clearly distinguishable. In Fig. 23(b), we see an intersonic crack around which the fringe pattern has been compressed severely in the direction parallel to the interface, with both the front lobe and the back lobes being shortened. However, the fringe pattern is elongated along the direction perpendicular to the interface. This distortion is probably due to the stress field induced by the loading pulse propagating through the Homalite. In Fig. 23(a), the loading waves are transmitted into the Homalite half indirectly through the interface and hence the crack tip fields are not so affected by the stresses induced by the loading pulse. Also in Fig. 23(b) we conjecture that the crack face frictional contact zone starts close to the crack tip after and infinitesimal traction-free zone and extends all the way up to the trailing Rayleigh singularity, as indicated by the numerous fringes parallel to the interface. This also results in the Mach wave emanating from the crack tip not being as sharp as in Fig. 23(a).

9. Summary

The primary goal of the experiments discussed in this paper was to carefully study the transition of a bimaterial interface crack from subsonic to intersonic speeds. An attempt was made to give clear physical arguments as to the nature of the subsonic/intersonic transition. Also, the effect of differing specimen geometry, loading configurations, and different bimaterial systems on the subsonic/intersonic transition and the crack propagation behavior was investigated.

Acknowledgements

The authors gratefully acknowledge the support of the National Science Foundation (Grant #CMS9813100 and Grant #CMS9983779) and of the Office of Naval Research (grant #N00014-95-1-0453, Dr. Y.D.S. Rajapakse, Project Monitor).

References

[1] Kanninen MF, O'Donoghue PE. Research challenges arising from current and potential applications of dynamic fracture mechanics to the integrity of engineering structures. Int J Solids Struct 1995;32(17–18):2423–45.
[2] Dmowska R, Rice JR. Fracture theory and its seismological applications. In: Teisseyre R, editor. Continuum theories in solid earth physics. Amsterdam: Elsevier; 1986. p. 187–255.
[3] Scholz CN. The mechanics of earthquakes and faulting. Cambridge: Cambridge University Press; 1990.
[4] Andrews DJ, Ben-Zion Y. Wrinkle-like slip pulse on a fault between different materials. J Geophys Res 1997;102(B1):553–71.
[5] Harris RA, Day SM. Effects of a low-velocity zone on a dynamic rupture. Bull Seismol Soc Am 1997;87(5):1267–80.
[6] Ranjith K, Rice JR. Slip dynamics at an interface between dissimilar materials. J Mech Phys Solids 2000;49(2):341–61.
[7] Adams GG. An intersonic slip pulse at a frictional interface between dissimilar materials. J Appl Mech 2001;68(1):81–6.
[8] Cochard A, Rice JR. Fault rupture between dissimilar materials: Ill-posedness, regularization and slip-pulse response. J Geophys Res 2000;105(B11):25891–907.
[9] Ben-Zion Y. Dynamic rupture in recent models of earthquake faults. J Mech Phys Solids 2001;49(9):2209–44.
[10] He MY, Hutchinson JW. Kinking of a crack out of an interface. J Appl Mech 1989;56:270–8.
[11] He MY, Bartlett A, Evans AG, Hutchinson JW. Kinking of a crack out of an interface—role of inplane stress. J Am Ceram Soc 1991;74(4):767–71.
[12] Hutchinson JW, Suo Z. Mixed-mode cracking in layered materials. Adv Appl Mech 1992;29:63–191.
[13] Goldshtein RV. Stationary motion of a crack along a straight bond line between two dissimilar materials. Mekhanika Tverdogo Tela 1966;1(5):93–102 [in Russian].
[14] Goldshtein RV. On surface waves in joined elastic materials and their relation to crack propagation along the junction. Appl Math Mech 1967;31(3):496–502.
[15] Willis JR. Fracture mechanics of interfacial cracks. J Mech Phys Solids 1971;19:353–68.
[16] Brock LM, Achenbach JD. Extension of an interface flaw under the influence of transient waves. Int J Solids Struct 1973;9:53–67.
[17] Atkinson C. Dynamic crack problems in dissimilar media. In: Sih GC, editor. Mechanics of Fracture: Elastodynamic Problems, vol. 4. Holland: Noordhoff; 1977. p. 213–48.
[18] Tippur HV, Rosakis AJ. Quasi-static and dynamic crack growth along bimaterial interfaces—A note on crack-tip field measurements using coherent gradient sensing. Experim Mech 1991;31(3):243–51.
[19] Yang W, Suo Z, Shih CF. Mechanics of dynamic debonding. Proc Royal Soc London A 1991;433(1889):679–97.
[20] Lambros J, Rosakis AJ. Development of a dynamic decohesion criterion for subsonic fracture of the interface between two dissimilar materials. Proc Royal Soc London A 1995;451(1943):711–36.
[21] Lambros J, Rosakis AJ. Dynamic decohesion of bimaterials—experimental observations and failure criteria. Int J Solids Struct 1995;32(17–18):2677–702.
[22] Kavaturu M, Shukla A. Dynamic fracture criteria for crack growth along bimaterial interfaces. J Appl Mech 1998;65(2):293–9.
[23] Liu C, Lambros J, Rosakis AJ. Highly transient elastodynamic crack growth in a bimaterial interface—higher order asymptotic analysis and optical experiments. J Mech Phys Solids 1993;41(12):1857–954.
[24] Lambros J, Rosakis AJ. Shear dominated transonic interfacial crack growth in a bimaterial. 1. Experimental observations. J Mech Phys Solids 1995;43(2):169–88.

[25] Singh RP, Lambros J, Shukla A, Rosakis AJ. Investigation of the mechanics of intersonic crack propagation along a bimaterial interface using coherent gradient sensing and photoelasticity. Proc Royal Soc London A 1997;453(1967):2649–67.
[26] Rosakis AJ, Samudrala O, Singh RP, Shukla A. Intersonic crack propagation in bimaterial systems. J Mech Phys Solids 1998;46(10):1789–813.
[27] Singh RP, Shukla A. Subsonic and intersonic crack growth along a bimaterial interface. J Appl Mech 1996;63(4):919–24.
[28] Liu C, Huang Y, Rosakis AJ. Shear dominated transonic interfacial crack growth in a bimaterial. 2. Asymptotic fields and favorable velocity regimes. J Mech Phys Solids 1995;43(2):189–206.
[29] Huang Y, Liu C, Rosakis AJ. Transonic crack growth along a bimaterial interface: an investigation of the asymptotic structure of near-tip fields. Int J Solids Struct 1996;33(18):2625–45.
[30] Yu HH, Yang W. Mechanics of transonic debonding of a bimaterial interface—the antiplane shear case. J Mech Phys Solids 1994;42(11):1789–802.
[31] Yu HH, Yang W. Mechanics of transonic debonding of a bimaterial interface—the inplane case. J Mech Phys Solids 1995;43(2):207–32.
[32] Yu HH, Suo Z. Intersonic crack growth on an interface. Proc Royal Soc London A 2000;456(1993):223–46.
[33] Brock LM. Interface crack extension at any constant speed in orthotropic or transversely isotropic bimaterials—i. General exact solutions, in press.
[34] Brock LM. Interface crack extension at any constant speed in orthotropic or transversely isotropic bimaterials—ii. Two important examples, in press.
[35] Huang Y, Wang W, Liu C, Rosakis AJ. Intersonic crack growth in bimaterial interfaces: an investigation of crack face contact. J Mech Phys Solids 1998;46(11):2233–59.
[36] Wang W, Huang Y, Rosakis AJ, Liu C. Effect of elastic mismatch in intersonic crack propagation along a bimaterial interface. Eng Fract Mech 1998;61(5–6):471–85.
[37] Xu XP, Needleman A. Numerical simulations of dynamic crack growth along an interface. Int J Fract 1996;74(4):289–324.
[38] Breitenfeld MS, Geubelle PH. Numerical analysis of dynamic debonding under 2-D in-plane and 3-D loading. Int J Fract 1998;93(1–4):13–38.
[39] Needleman A, Rosakis AJ. The effect of bond strength and loading rate on the conditions governing the attainment of intersonic crack growth along interfaces. J Mech Phys Solids 1999;47(12):2411–49.
[40] Lambros J. Dynamic decohesion of bimaterial interfaces, PhD thesis, California Institute of Technology, Pasadena, CA, USA, 1994.
[41] Singh RP. Catastrophic failure of bimaterial interfaces, PhD thesis, University of Rhode-Island, Kingston, RI, USA, 1995.
[42] Dally JW, Riley WF. Experimental stress analysis. New York: McGraw-Hill; 1991.
[43] Rosakis AJ. Two optical techniques sensitive to gradients of optical path difference: the method of caustics and the coherent gradient sensor. In: Epstein JS, editor. Experimental techniques in fracture. New York: VCH; 1993, p. 327–425.
[44] Kalthoff JF. Shadow optical analysis of dynamic shear fracture. Proceedings of the International Conference on Photomechanics and Speckle Metrology, SPIE, vol. 814, 1987. p. 531–8.
[45] He MY, Hutchinson JW. Crack deflection at an interface between dissimilar elastic-materials. Int J Solids Struct 1989;25(9):1053–67.
[46] Liechti KM, Chai YS. Biaxial loading experiments for determining interfacial fracture toughness. J Appl Mech 1991;58(3):680–7.
[47] Xu LM, Tippur HV. Fracture parameters for interfacial cracks—an experimental—finite element study of crack-tip fields and crack initiation toughness. Int J Fract 1995;71(4):345–63.
[48] Rosakis AJ, Samudrala O, Coker D. Cracks faster than the shear wave speed. Science 1999;284(5418):1337–40.
[49] Singh RP, Shukla A. Characterization of isochromatic fringe patterns for a dynamically propagating interface crack. Int J Fract 1996;76(4):293–310.
[50] Freund LB. The response of an elastic solid to nonuniformly moving surface loads. J Appl Mech 1973;40:699–704.
[51] Schallamach A. How does rubber slide? Wear 1971;17:301–12.
[52] Adams GG. Dynamic instabilities in the sliding of two-layered elastic half-spaces. J Tribol 1998;120(2):289–95.
[53] Kobayashi AS, Mall S. Dynamic fracture toughness of homalite-100. Exp Mech 1978;18:11–8.